Fatigue crack growth in inhomogeneous steel components

Fatigue crack growth in inhomogeneous steel components

D. Firrao, P. Matteis, P. Russo Spena, G.M.M. Mortarino

Dip. di Scienza dei Materiali e Ingegneria Chimica, Politecnico di Torino, Torino, Italy

Keywords: fatigue crack-growth simulation; low-alloy quenched and tempered steel; mixed microstructure; crack shape evolution.

ABSTRACT

Massive low-alloy high-strength steel components often exhibit microstructure variations from surface to core due to decreasing cooling rates when moving towards the interior. Since different steel constituents exhibit different Fatigue Crack Growth (FCG) behaviors, both the overall and local FCG rates are expected to be influenced by the microstructural changes, that in turn affects the crack shape.

The case of slack-quenched components with simple geometries, having a surface flaw, and subjected to constant-force-amplitude tensile fatigue, is first examined theoretically. The microstructural variations are hypothesized by considering low-alloy steel hardenabilities and medium quench severities; thereafter, the FCG is computed by considering (during each integration step) the stress-intensity-factor amplitude and the FCG behavior of different points of the crack front, the pointwise FCG properties being determined by the local steel constituents fractions.

Simulation results are compared with experimental evidences from a recent failure in a 90 mm diameter low-alloy steel connection rod of a 2460 kW naval diesel generator.

INTRODUCTION

The application of Paris relationship [1] helps solving many practical problems in the case of large components in which Non Destructive Testing (NDT) discovers an active crack which is slowly fatigue propagating while the plant is still in operation. The precise knowledge of the coefficients to be inserted in the relationship allows to correctly estimate the time required to reach the unsafe operations stage and to decide if there is ample space to order, fabricate and commission a new component. Electricity generation or chemical plants, steel mills, oil drill derricks are among the most common industrial systems where the Paris relationship can be of use.

The case of components with homogeneous microstructures and simple geometries, having a surface flaw, and subjected to constant-force-amplitude tensile fatigue, has been broadly analyzed, whereas very few papers examine fatigue crack propagation in inhomogeneous microstructures.

Calculations based on the relationship can be affected by large degrees of error because, in large steel components, the knowledge of the microstructure as produced by the actual heat treatment during fabrication is scarce or not considered; hence, standard average coefficients, as commonly inserted in widely used codes, are used. Yet, in large components there is always a variation of microstructures along the cross section, even if high hardenability steel grades are used. Thus, simulation results may at times be largely deceptive.

Whereas tempered martensite is almost always predominating in a medium carbon low-alloy steel component surface layer, mixed microstructures encompassing first tempered bainite and then pearlite are present at increasing distance from the surface. Moreover, a mostly pearlitic structure can be present at core. Both at mid-depth and at core, pearlite can be at times accompanied by a thin ferrite network. Finally, in nickel or medium manganese alloyed steels, residual austenite is always present after quench and its presence can be detected as “transformed” islands after tempering. A multilaboratory in-depth testing campaign has allowed first to assess microstructure and mechanical properties variations in large quenched and tempered steel blooms for large plastic components dies of the ISO 1.2738 grade [2] and then to determine coefficients to be inserted in the Paris relationship in correspondence of various types of microstructures [3,4].

In the case of components smaller than dies for plastic pieces, but still rather massive, less alloyed steel grades may be employed, with similar microstructures encountered at increasing depths. The possibility of using the same Paris relationship coefficients, as determined in die steels, even if the chemical compositions of individual phases forming the same metallographic constituents is different, is here hypothesized. In fact, the presence of less chromium or manganese

in the cementite-type carbides of pearlite, or of less chromium, manganese, or nickel in ferrite network or ferrite pearlitic lamellae and ferrite present in tempered martensite is deemed not to strongly influence overall fatigue crack growth velocities. In fact, cementite lamellae are inherently brittle and always break before the surrounding ferrite lamellae or small crystals, which then controls the FCG rate. Constrained ductility prevents Ni or Mn from fully developing their strengthening contribution to ferrite.

The effect of a variation of the Paris law parameters, due to a microstructural gradient, upon the fatigue growth of a surface crack through the section of a large steel component, is discussed here on the basis of Fatigue Crack Growth (FCG) calculations, performed in the case of either a slab or a round bar loaded in alternating tension. The crack front is assumed to be an arc of ellipse at all stages of growth, whereas the above-mentioned microstructure-dependent Paris coefficients and literature formulas for calculating the Stress Intensity Factor (SIF) values are applied in two different points along the crack front; the deepest (most far from the surface) SIF calculation point encounters varying microstructures as the crack grows. The latter results are compared with observations performed on a low-alloy quenched and tempered steel connection rod, which underwent a fatigue failure while being employed with almost constant stress cycles. Differences induced by the concurrency of the plane stress condition at the periphery of the bar or the slab and of the plane strain condition elsewhere do not reflect on the final rupture, which occurs when the applied SIF in plane strain condition reaches the fracture toughness pertaining to the local micro-constituent.

EXPERIMENTAL

The examined connection rod was mounted in a 6 cylinders, 2460 kW electricity diesel generator motor, having a constant crankshaft rotation velocity of 750 rotations/minute. The fracture occurred at the stress concentration determined by the intersection of the grossly conical portion and the central cylindrical portion of the component, where the diameter is ~90 mm, with a 15 mm diameter coaxial lubrication hole (Fig. 1). The cracked section is nearly perpendicular to the loading axis (which is horizontal in Fig. 1).

The connection rod undergoes one fatigue cycle every two crankshaft rotations: the maximum compressive stress occurs during the power stroke, whereas the maximum tensile stress occurs during the intake stroke, mainly due to inertial forces, and is estimated by FEM calculations to reach a maximum of 70 MPa in 20% overspeed periods and 50 MPa during normal operations.

The connection rod was fabricated from a medium-carbon low-alloy steel classifiable under the AISI 4135, or EN 34CrMo4 steel standards, further micro-alloyed with B (Table. 1).

On the basis of the steel composition and consequent ideal critical diameter for hardening [5], a fully martensitic microstructure could be expected after an oil quench throughout the section of the connection rod. However, probably

due to the large heat content of the surrounding heavy portions, the metallurgical analysis of a rod cross-section, parallel to the cracked section and less than 20 mm away, showed that the hardness decreases, from $HV_{0.5}$ equal to 280 ca. at the surface to a 240-245 value at about 30 mm depth; concurrently the changes in the microstructure (as observed by optical microscopy) become more pronounced at a depth of 30 mm from the surface. The surface microstructure consists of a homogeneous dispersion of submicron carbides in a ferritic matrix, which is interpreted as martensite tempered slightly above 650 °C taking also into account hardness readings. Increasing limited areas of "tempered" bainite occur alongside the tempered martensite as the distance from the outer circumference increases. Finally, even if tempered martensite and/or bainite are still prevalent, the increasing presence of prior austenite grain borders thin ferrite networks and dispersed coarse and fine pearlite colonies was recognized beyond 22 mm depth, to reach almost half of the microstructure at a 30 mm depth (Fig. 2). The metallographic findings are further complemented by tensile properties: one longitudinal tensile specimen machined from the fractured connection rod exhibited an ultimate tensile strength of 770 MPa, whereas a value of 980 MPa ca. could be expected from this steel after tempering at 650 °C, if a completely martensitic microstructure had been achieved upon quenching [5, 6].

Even if parts of the fracture surfaces were damaged during the crankshaft rotations successive to failure, the fractographic analysis showed that the FCG ascribable to the Paris regime started from a surface crack at least 4 mm deep having an almost straight crack front, and extended up to about 42 mm depth, and that the final (overload) rupture occurred once the crack had just reached the central portion of the lubrication hole. Variations in the appearance of the fatigue fracture surface were seen starting from a 28 mm depth (Figs. 3a and 3b): in Fig. 3b the crests of subsequent ferrite lamellae are evident with fine fatigue markings. They constitute the comb of resisting platelets once the cementite crystals have failed for excessive strain in the plasticized region ahead of the crack tip. The final overload fracture was microscopically ductile exhibiting microvoid coalescence (Fig. 4). Areas where constrained ductility microvoids could be found were observed at core (Fig. 4b); these latter microvoids were either less deep, or more elongated in section, or both, than those found in the outer ring overload fracture area (Fig. 4a).

CALCULATIONS

The calculations consider an edge crack in a plate or in a round bar, lying in a plane perpendicular to the free surface and to the loading axis. The plate thickness B and the bar diameter D are equal to the nominal diameter of the connection rod. The crack is the intersection of an ellipse centered at the bar (or plate) surface with the bar (or plate) itself, hence it is described by the ellipse semiaxes a and b, the former being perpendicular to the free surface. In both cases a is also the maximum depth of the crack front. In the plate b is also the crack half-width on the free surface, whereas in the round bar the crack circumferential half-width on the free surface is named c. (Fig. 5).

The initial crack is assumed to be 4 mm deep and to have an aspect ratio $a/b = 0.18$, similar to the initial defect of the connection rod. The bars are loaded with a constant tensile stress amplitude $\Delta\sigma = 50$ MPa, equal to the maximum estimated tensile part of the normal loading cycle of the connection rod (since the compression portion of a load cycle does not contribute to FCG). Hence, the *R* ratio (ratio of the minimum and maximum load) is assumed to be zero.

The FCG calculations are performed by repeating the following steps:

(i) the FCG rates da/dN and dc/dN are computed in the points *A* and *C* of the current crack front, where *A* is the deepest point and *C* is a point close to the outer surface; (ii) an incremental step ΔN of the total number of cycles *N* is chosen to yield ~0.2 mm crack length increments; (iii) the points *A* and *C* are advanced in the direction perpendicular to the crack front by the distance determined by $\Delta N \cdot da/dN$ and $\Delta N \cdot dc/dN$, respectively; (iv) the semiaxes *a* and *b* of the new crack front are calculated by imposing that the new ellipse passes trough the new *A* and *C* points.

The material is described by pointwise fractions of metallurgical constituents, determined by progressive optical metallography comparisons; different Paris law parameters pertaining to each, the FCG rate in a point is computed as the weighted average of the FCG rates of each constituent, as obtained by the relevant Paris plot upon considering the cyclic amplitude ΔK of the Stress Intensity Factor (SIF).

The elliptic-arc crack model is chosen because previous works showed that it is a fair approximation of the shape of growing surface cracks in both rectangular [7] and round [8] bars, regardless of the shape of the original flaw, and because it allows employment of literature formulas, obtained from past FEM analyses [9,10], to calculate the SIF and hence the FCG rate in the points *A* and *C* [7,9,10].

Since the larger cyclic plastic zone arising at the free surface (due to the local plane stress condition) is known to influence the local FCG behavior, in the case of the plate the FCG rate dc/dN of the free-surface C point is multiplied by 0.9, as suggested by the previous literature [7,9], whereas in the round bar the same problem is avoided by choosing the *C* point at a suitable distance from the free surface, as described in reference [10].

This two-point FCG calculation procedure allows the crack aspect ratio to vary as a consequence of the two different pointwise FCG rates, which in turn depend on the local ΔK and microstructure. During FCG, point *A* moves towards the bar core, whereas point *C* moves along the bar surface, so that the FCG rate in these two points is differently influenced by the bar microstructure, which can dictate not only the average FCG rate, but also the crack aspect ratio.

The fraction of tempered martensite is assumed to be 1 at depth ≤ 22 mm, to decrease linearly between 22 and 34 mm depth, and to be 0 at depth ≥ 34 mm; the rest is assumed to be pearlite. This choice is based on the hypothesis that, once the fatigue crack encounters a mixed microstructure with thin ferrite areas and pearlite, its growth is progressively retarded by the more resistant constituent (ferrite); hence it can be modeled by the pearlite FCG behavior as if it were

growing in a fully pearlitic microstructure. Calculations of the FCG inside homogeneous tempered martensite plates or bars are also performed for comparison, everything else being equal.

The FCG rate is computed with the Paris relationship $da/dN = C \cdot \Delta K^m$ and the following material parameters, obtained from previously published Paris plots with an R ratio of 0.1 [3,4]: $C = 1.35 \cdot 10^{-11}$ [m·(MPa√m)$^{-m}$] and $m = 2.8$ for tempered martensite in the 5 to 70 MPa√m ΔK range; $C = 7.15 \cdot 10^{-13}$ [m·(MPa√m)$^{-m}$] and $m = 3.4$ for pearlite in the 5 to 45 MPa√m ΔK range. The corresponding Paris plots are shown in Fig. 6. These relationships were extrapolated when only one of the two calculation points exhibit a SIF value lower than 5 MPa√m.

The FCG calculations were stopped once the crack depth a exceeds 44 mm, because such a crack size roughly corresponds to the final one observed in the connection rod case, and because in the point A of the partially pearlitic round bar the same crack size causes ΔK to slightly exceed 45 MPa√m, which is the upper limit of the employed pearlite Paris law, and implies that the maximum SIF value becomes close the estimated pearlite fracture toughness.

RESULTS

The results of the four FCG calculations, with either the plate or the round bar geometry, and with either the homogeneous tempered martensite microstructure or the above described microstructural gradient with pearlite at core, are compared in Figs. 7 to 11 for the case of 50 MPa maximum stress.

The SIF values are always lower in the plate case, owing to the plate being assumed infinitely wide.

In the plate case the total number of cycles increases approximately from 5 to 6.5 million due to the presence of pearlite at core (Fig. 7). In the round bar case, the total number of cycles is about 4 million in the total tempered martensite hypothesis and increases slightly if pearlite is hypothesized, because when the crack encounters the pearlitic region the SIF values and hence the FCG rates are already comparatively high (Fig. 8).

In both the plate and the round bar cases the crack shape (Figs. 9 to 11) is greatly influenced by the microstructure. If the material is homogeneous, the a/b ratio, which was assumed to be low at the beginning of the FCG, first increases in both the plate and round bar cases, then continues to increase at a lower pace in the plate case, whereas it exhibits a blunt maximum at about $a/D = 0.3$ in the round bar case (Fig. 9). This is consistent with previous numerical and experimental results for similar initial a/b value for both plates [7] and round bars [10,11]. On the contrary, if the microstructure is not homogeneous, once the crack depth a reaches the microstructural transition region at 22 to 34 mm depth, the a/b ratio first exhibit a maximum and then starts to decrease, and continues with this latter trend until the end of the calculation. In the plate case, this implies that in the final stage the crack half-width b increases much more than the crack depth (Fig. 10), while in the round bar case the crack front becomes almost straight again (Fig. 11). Fig. 12 shows the actual situation in the 90 mm round bar. Calculations performed with a 40 MPa maximum tensile stress show

that the total number of cycles before fracture obviously increases, but differences due to microstructure variations are similar to the 50 MPa case, including the aspect ratios.

CONCLUSIONS

The study stems from previous observation that different steel constituents exhibit notably different FCG behaviors [3,4]. To investigate consequences, the crack propagation of an elliptical defect in a plate or in a round bar characterized by a microstructural gradient from surface to core was simulated and compared with observations of a recent service failure occurred in a 90 mm diameter connection rod of a 2460 kW naval diesel generator.

The FCG was calculated in two independent points on the crack front using literature SIF solutions. More accurate calculation could be performed by considering more than two independent points on the crack front, allowing description of the crack shape by more than two geometrical parameters, but requiring calculation of the SIF values by FEM at each step [12]. However, the present two-point method was adequate to illustrate the possible influence of the steel microstructure upon the FCG, and its results were compatible with the above mentioned observations.

It was found that a microstructural gradient can cause a large variation in the crack shape, even if the underlying difference in the FCG behavior is not large. In particular, it was found that the presence of pearlite at core can cause a flattening of the crack front when it reaches the core itself.

The latter finding was compatible with the fractographic analysis of the above mentioned connection rod and it can be used as fractographic proof of the occurrence of an inhomogeneous microstructure in failure analysis situations, in the case of tensile fatigue of quenched and tempered steel components.

REFERENCES

[1] P. C. Paris, F. Erdogan. “A critical analysis of crack propagation laws”, J. Bas. Eng. Trans. ASME, series D, 85 (1963), 528-534.

[2] D. Firrao et al. “Relationships between tensile and fracture mechanics properties and fatigue properties of large plastic mould steel blocks”, Mater. Sc. Eng. A, 468-470 (2007), 193-200.

[3] D. Firrao et al. “Fatigue behavior of homogeneous-microstructure and mixed-microstructure steels”, In: Plasticity, failure and fatigue in structural materials - from macro to nano: proceedings of the Hael Mughrabi honorary symposium, TMS Annual Meeting & Exhibition 2008, 175-180.

[4] D. Firrao et al. “Fatigue behavior of homogeneous-microstructure and mixed-microstructure steels”, In: Multilevel Approach to Fracture of Materials, Components and Structures, VUTIUM (CZE), 17th European Conference on Fracture, 2008, pp. 2357-2363.

[5] ASTM A255-02, Standard Test Method for Determining Hardenability of Steel.

[6] R.A Grange, C.R. Hribal, L.F. Porter. “Hardness of tempered martensite in carbon and low-alloy steels”. Met. Trans. A, 8A (1977), 1775-1785.

[7] D. M. Shuter, W. Geary. “Fatigue crack growth from two-dimensional surface defects”, Fatigue Fract. Eng. Mater. Struct., 18 (1995), 653-659.

[8] R.G. Forman, V. Shivakumar. “Growth behavior of surface cracks in the circumferential plane of solid and hollow cylinders”, In: J.H. Underwood et. al. (eds.), Fracture Mechanics, 17th vol., ASTM STP 905, ASTM, Philadelphia, USA, 1986, pp 59-74.

[9] J.C. Newman Jr., I.S. Raju. “An empirical stress-intensity factor equation for the surface crack”, Engnr. Fract. Mech., Volume 15 (1981), 185-192.

[10] An. Carpinteri. “Shape change of surface cracks in round bars under cyclic axial loading”, Int. J. Fatigue, 15 (1993), 21-26.

[11] An. Carpinteri, R. Brighenti. “Part-through cracks in round bars under cyclic combined axial and bending loading”, Int. J. Fatigue, 18 (1996), 33-39.

[12] X. B. Lin, R. A. Smith. “Fatigue growth simulation for cracks in notched and unnotched round bars”, Int. J. Mech. Sci., 40 (1998), 405-419.

FIGURE CAPTIONS

Fig. 1. Drawing of the examined connection rod.

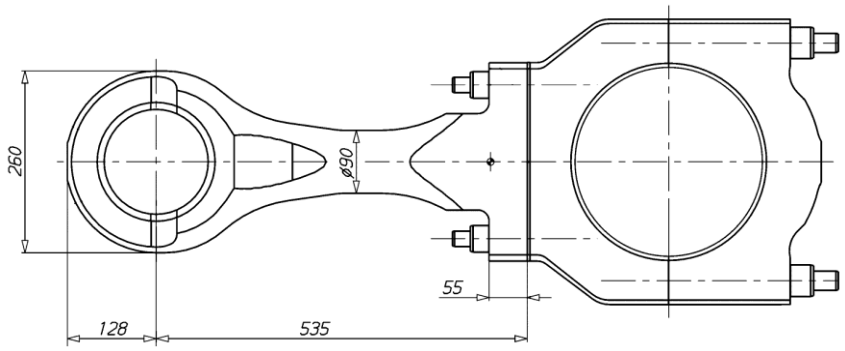

Fig. 2. Microstructure of the connection rod. A thin ferrite network surrounds islands of tempered pearlite and tempered bainite (1% Nital etch); 27 mm depth.

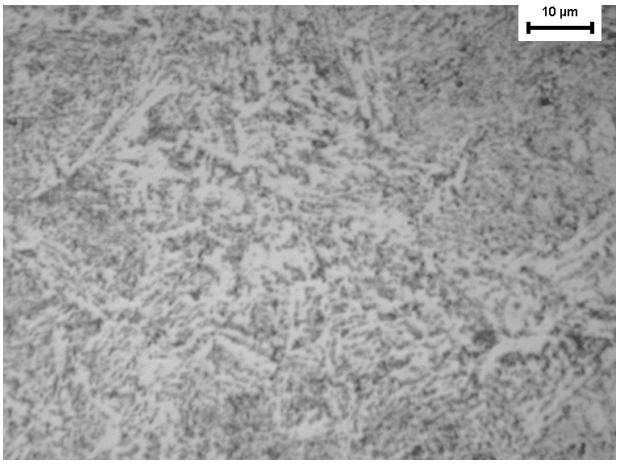

Fig. 3. Fatigue fracture surface in the homogeneous tempered martensite outer circular ring (a) and in the inhomogeneous inner ring, where tempered pearlite is present alongside ferrite and tempered bainite (b).

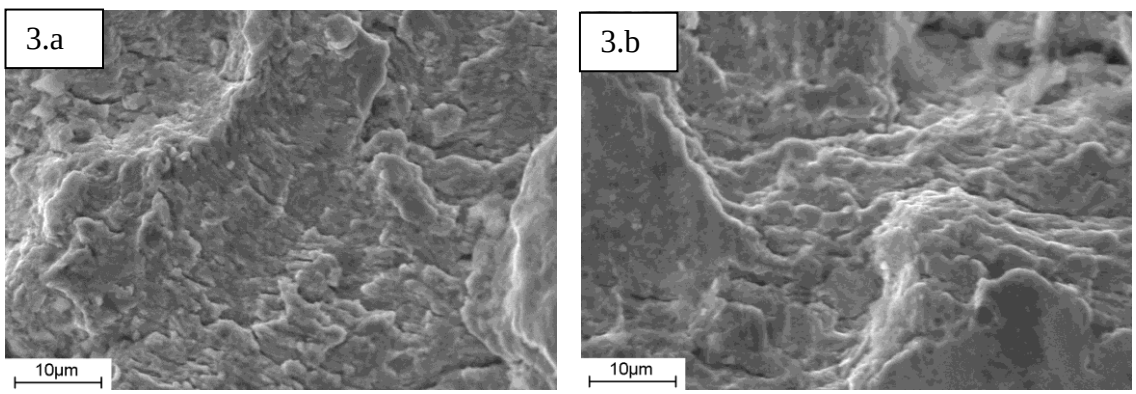

Fig. 4. Final fracture surface of the connection rod. Microvoid coalescence (a,b); pseudo-spherical dimples in the homogeneous tempered martensite outer ring (a); shallow and elongated dimples at the mixed microstructure inner ring (b).

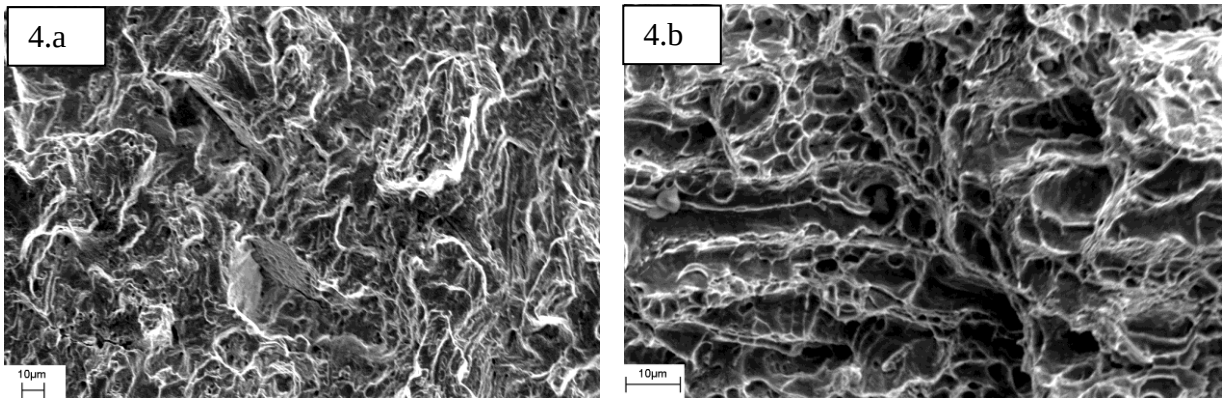

Fig. 5. Schematic diagram of the cracked cross section of the plate and of the round bar.

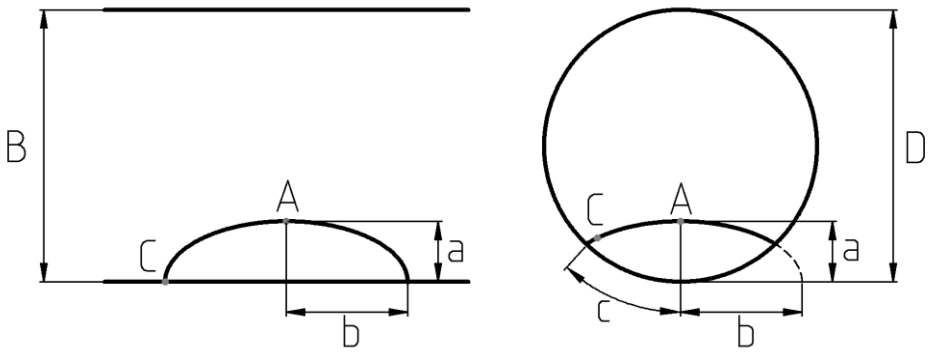

Fig. 6. Paris plot of the steel constituents, as employed in the FCG calculations.

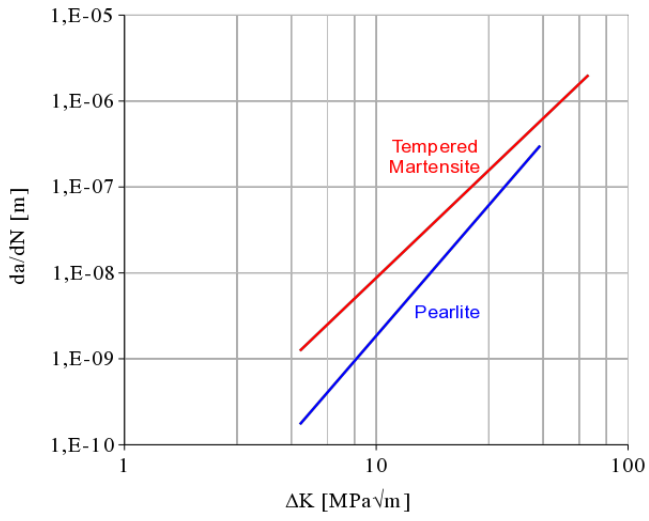

Fig. 7. Calculated fatigue growth of the crack depth *a* and of the crack half-width *b* in the plate, either with homogeneous tempered martensite microstructure or exhibiting pearlite at core.

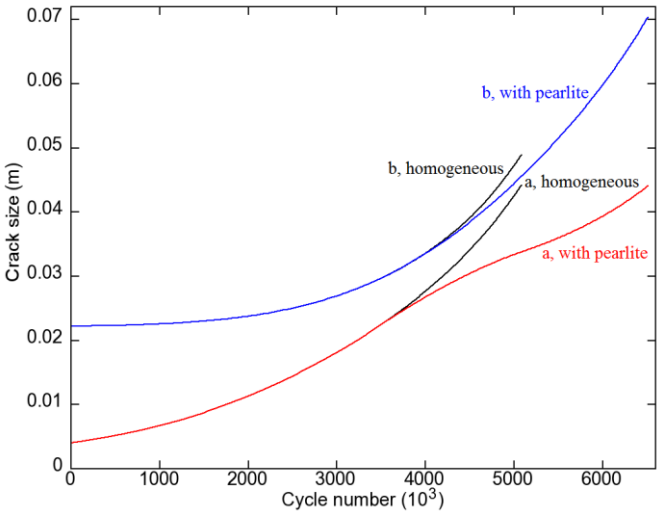

Fig. 8. Calculated fatigue growth of the crack depth *a* and of the crack circumferential half-width *c* in the round bar, either with homogeneous tempered martensite microstructure or exhibiting pearlite at core.

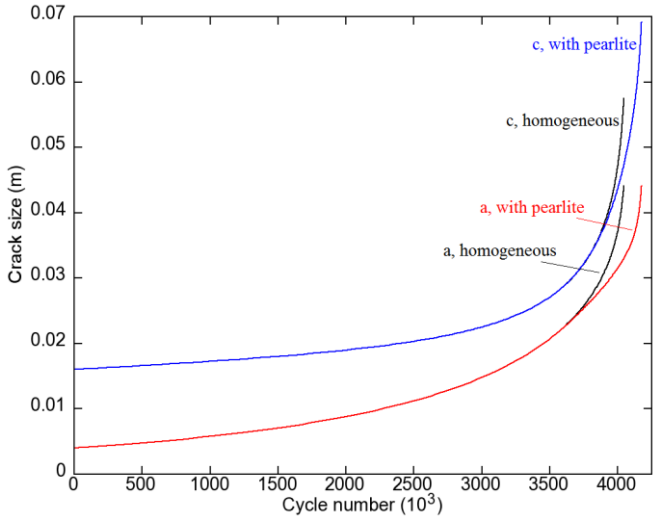

Fig. 9. Calculated crack shape aspect ratio in the plate and in the round bar, either homogeneous or exhibiting pearlite at core, as a function of relative crack depth.

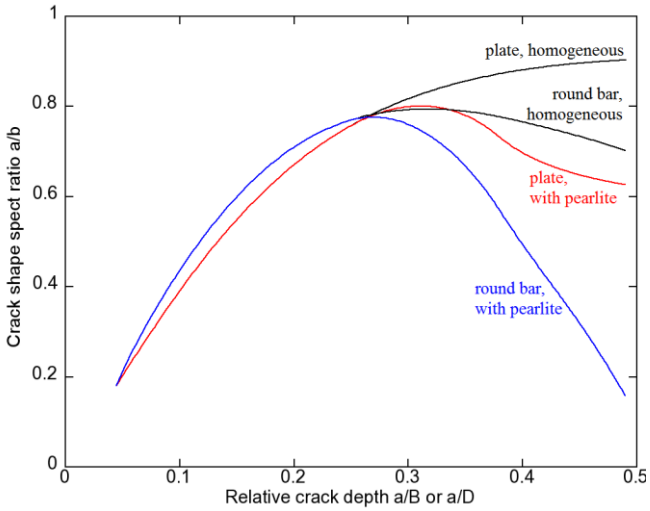

Fig. 10. Calculated crack geometry at selected cycle numbers in the plate, either with homogeneous tempered martensite microstructure (a) or exhibiting pearlite at core (b).

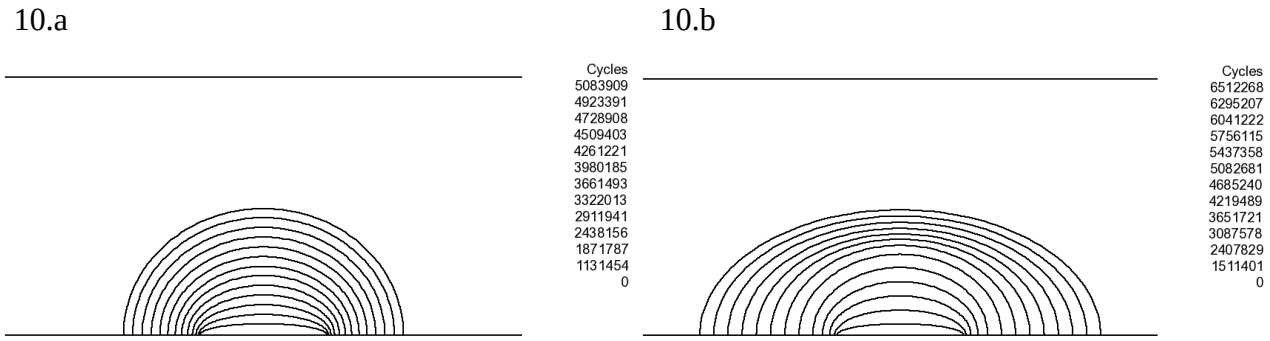

Fig. 11. Calculated crack geometry at selected cycle numbers in the round bar, either with homogeneous tempered martensite microstructure (a) or exhibiting pearlite at core (b).

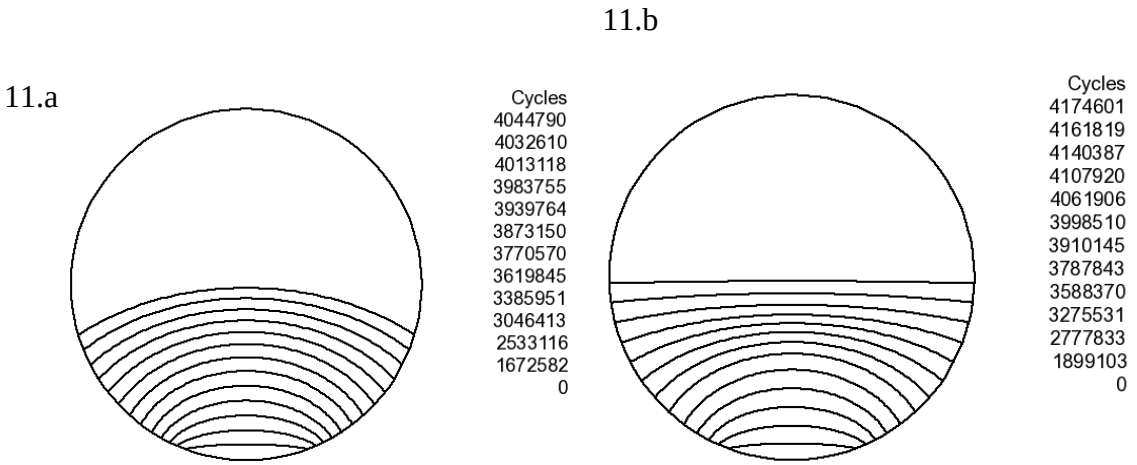

Fig. 12. Actual fractured section of the 90 mm dia. connecting rod with superimposed crack front lines (the dotted lines outline the undamaged fracture area).

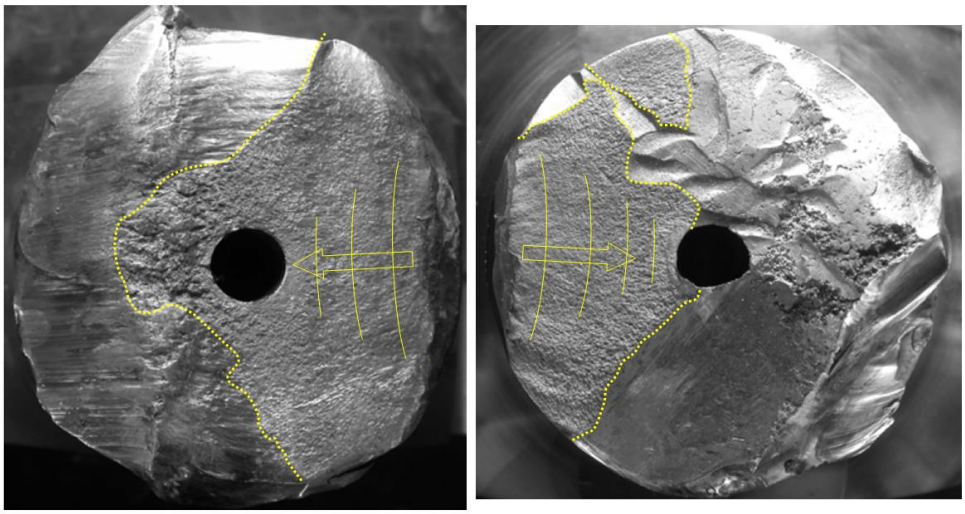

TABLES

Table. 1. Chemical composition of the connection rod steel (wt. pct.)

C	Mn	Si	P	S	Cr	Ni	Mo	Al	B
0.36	0.62	0.26	0.012	0.022	1.14	0.25	0.25	0.034	0.001